A synthetic platform for multiplex screening of cell-cell communication between soil fungi

Giovanni Schiesaro,[1] Agustina Undabarrena,[1] Mathies B. Sørensen,[2] Marcus Wäneskog,[1] Mathias Jönsson,[1] Ricardo Tenente,[3] Daniela Rago,[1] Marcus Deichmann,[1] Emma E. Hoch-Schneider,[1] Vijayalakshmi Kandasamy,[1] Emre Özdemir,[1] Pablo Cruz-Morales,[1] Thomas M. Frimurer,[3] Line Clemmensen,[2] Michael K. Jensen,[1] Emil D. Jensen[1,*]

[1] Novo Nordisk Foundation Center for Biosustainability, Technical University of Denmark, DK-2800 Kgs. Lyngby, Denmark

[2] Technical University of Denmark, Department of Applied Mathematics and Computer Science, Kgs. Lyngby, 2800, Denmark

[3] Novo Nordisk Foundation Center for Basic Metabolic Research, Faculty of Health and Medical Sciences, University of Copenhagen, Copenhagen, Denmark

* To whom correspondence should be addressed:

Emil D. Jensen, e-mail: emdaje@biosustain.dtu.dk

Abstract

Fungi are essential members of natural ecosystems and industrial biotechnology, yet they also pose significant risks to crops and human health. To thrive in microbial consortia a fungal organism must integrate the perception of both inter- and intra-species signals from the environment. Here we present a Yeast Mating Platform (YeMaP) to decipher cell-cell communication between fungal G protein-coupled receptors and short pheromone peptides. We use YeMaP to investigate the influence of abiotic factors on cell-cell communication in multiplex and for high-throughput screening of natural and synthetic pheromones to identify peptides with either improved potency or antagonism action. Additionally, we demonstrate that the plant pathogen *Fusarium oxysporum* possesses a robust cell-cell communication mechanism, which can, however, be disrupted by supplementing pheromones to promote

the communication of non-pathogenic organisms. Taken together, we envision that YeMaP could be applied to uncover the complexity of fungal communication and lead the application of future crop pest- and disease-management programs.

Introduction

Fungi are indispensable for fundamental processes of our global ecosystem such as the cycling of carbon, nitrogen, and phosphorus, which are all critical elements for the survival of plants and animals[1]. At the same time, pathogenic fungi pose an increasing threat to human health[2] and global food security[3]. As climate change intensifies, the available data and simulation models indicate that plant disease pressures are likely to rise substantially[4].

To address these emerging challenges we need a greater understanding of how intra- and interspecies communication occurs in fungal consortia. G protein-coupled receptors (GPCRs) are the master switches that convert external stimuli into an internally coordinated cellular response[5]. Through GPCRs, fungi can detect various chemical signals, including pheromones, nutrients, ions, hydrophobic surfaces, and even light, allowing them to regulate their development, metabolism, and virulence[6]. However, the current understanding of fungal GPCRs is limited[6], and the interaction between receptors and ligand(s) is often poorly understood, which hinders the development of new antifungal drugs and sustainable pest management systems for agriculture[7,8].

The model yeast *Saccharomyces cerevisiae* encodes three GPCRs, two of which are mating receptors, *STE2* and *STE3* expressed in *MAT***a** and *MAT*α cells, respectively[9]. To form diploid cells, the haploid *MAT*α cells communicate through an unmodified short peptide (α-factor) to *MAT***a** cells, which respond with a post-translationally modified peptide (**a**-factor)[10]. In contrast, in the asexual plant pathogen *Fusarium oxysporum,* the autocrine pheromone communication regulates the conidial germination[11], and the GPCR receptor

STE2 is involved in the chemotropism toward plant roots[12]. A similar mechanism has recently been shown in *Fusarium graminearum*[13] highlighting a new role for mating receptors and posing the question of a possible conserved mechanism of plant recognition among soil fungi. Fungal mating receptors have been extensively expressed in *S. cerevisiae* for pathogen detection[14] or to establish orthogonal communication[15] in biosensor strains. Cell-cell communication between GPCRs and pheromones in multiplex assays has never been tested to mimic the presence of multiple fungal organisms, although it more closely resembles the conditions for real-world soil microbiome interactions. Additionally, fungal pheromones share some degree of conservation among closely related species[16] and can be involved in interspecies communication[17], which suggests that yeast mating is a suitable tool to study fungal cell-cell communication.

Unlike biosensors based on GPCRs[18], successful mating requires the secretion and detection of pheromones along with the appropriate induction of a cell program for fusion at the cellular and nuclear levels[19].

Here, we describe a yeast mating platform (YeMaP) for studying interactions between fungal GPCRs and pheromones. YeMaP enabled us to study fungal communication from four different perspectives: i) the interaction between a GPCR and a pheromone, ii) the screening of a library of pheromone variants for identification of a synthetic pheromone with higher potency against *F. oxysporum* Ste2, iii) modeling fungal cell-cell communication within consortia, and iv) assessing the effects of abiotic factors - such as pH, different nitrogen sources, the presence of a plant peroxidase, or external pheromones - on a network of library-on-library interactions.

Results

Engineering yeast mating to study GPCR-pheromone interactions (One-on-One) and to predict real-life fungal interaction.

To define the best design for establishing a synthetic platform for studying network interactions among multiple fungal GPCRs, we initially focused on two GPCRs from *Candida albicans* (*Ca*) and *Fusarium graminearum* (*Fg*), which had previously been expressed in yeast[15,22,23], each co-cultured with a strain expressing the cognate pheromone (Fig. 1A). Since asymmetry in sexual pheromones is not required between yeast mating pairs[24], we sought to identify which combination of mating-types would be more suitable for GPCR substitutions and pheromone production[25]. By co-culturing the two different designs, followed by growth-based diploid selection, we found that the substitution of Ste3 in *MAT*α cells and the production of the fungal pheromone in *MAT***a** cells allowed for the highest diploid frequencies, a result in line with Huberman et. al[26] (Fig. 1B). For the *Ca* pair, in particular, we observed a 33-fold difference between the two mating-types ($p<0.0001$) (Fig. 1B). Next, to assess if mimicking native pheromone expression dynamics is an essential feature[10,22], we tested constitutive vs. inducible expression of the cognate heterologous pheromone and scored the resulting diploid frequencies. Although we observed increased diploid frequencies when heterologous pheromones were expressed from the inducible *MFA2* promoter[27] compared to the strong constitutive *TDH3* promoter[28], statistical significance was only achieved when the strains were deleted for both **a**-factor genes, *MFA1* and *MFA2* ($p=0.039$ with *Ca*.Ste2 and $p=0.005$ with *Fg*.Ste2) (Fig. 1C). Importantly, we did not observe diploid formation when a GPCR strain was co-cultured with a non-cognate pheromone expressing strain (Fig. 1C).

Having established the optimal strain design above, we cross-evaluated the specificity of our platform by performing a “One-on-One” mating matrix in deep well plates between a library consisting of 10 GPCRs and 10 cognate pheromones (Fig. 1D). Here we observed the promiscuity of *Beauveria bassiana* (*Bb*) GPCR (*Bb*.Ste2) towards *Fusarium oxysporum (Fo)*, and *Hypocrea jecorina* (*Hj)* pheromones, and the induction of diploid formation when *Fo* pheromone was co-cultured with *Fg*.Ste2, *Fo*.Ste2, or *Bb*.Ste2. (Fig. 1D). To validate these results, we selected 4 mating receptors (*Fg*.Ste2, *Fo*.Ste2, *Bb*.Ste2, and *Botrytis cinerea* - *Bc*.Ste2) and their cognate pheromones and performed biosensor assays in parallel to

mating-based selection in culture tubes. We observed a binary (on/off) behavior for the biosensors, in particular, almost full activation of the pheromone response pathway in *Bb*.Ste2 with *Fg* pheromone, and the highest activation in *Fo*.Ste2 when co-incubated with *Bb* pheromone (Fig. 1E). The same two interactions with our Yeast Mating Platform (YeMaP) did not translate into a similar level of diploid formation compared to the cognate pheromone interaction. The validation of the mating matrix in culture tubes recapitulated the same trends as in **Fig. 1D**, yet with a higher diploid frequency (Fig. 1F).

As a consequence of the confirmed cross-reactivity between *Bb*.Ste2 and *Fo* pheromone, along with the documented protective effect of *Bb* against *Fo* on crops[29,30], we investigated, in the real organism, if *Bb* could detect *Fo* pheromone. Both *Bb* and *Fo* pheromones at a concentration of 378 μM induced a positive spore chemotropism ($p<0.05$ and $p<0.05$), while a scrambled version of the *Fo* pheromone did not (Supplementary Fig. 1). To further explore the role of *Bb*, *Fo* or scrambled pheromones on *Bb* metabolism, we cultivated *Bb* with individual peptide supplementation and performed a metabolomic analysis (see Method section). We first conducted a targeted analysis on 25 secondary metabolites described in the literature[31,32] (Supplementary Table 3), however, these metabolites did not show any condition-specific correlation. Using ANOVA simultaneous component analysis (ASCA[33]), we found that individual pheromone supplementations produced significantly distinct metabolic profiles, primarily for hydrophobic compounds detected when method B was applied (see Methods section and Supplementary Fig. 2A). To further explore this vast chemical diversity, we applied MzMine[34] for processing followed by feature-based molecular networking[35]. Although most of the features responsible for the separation were singletons, we found that beauvericin and all the masses present in its fragmentation network were co-responsible for the separation in the ASCA plot for the Principal Component 1 (PC1), consistent with the increased production in structurally related molecules, such as Beauvericin A, D and Beauvenniatin A when *Bb* pheromone was supplemented (Supplementary Fig. 2B-G).

In summary, we have established a synthetic platform to further investigate cell-cell communication based on isolated fungal GPCR and pheromone. We further validated that *Bb* can sense *Bb* and *Fo* pheromones and that these two pheromones induced distinct metabolic profiles in *Bb*.

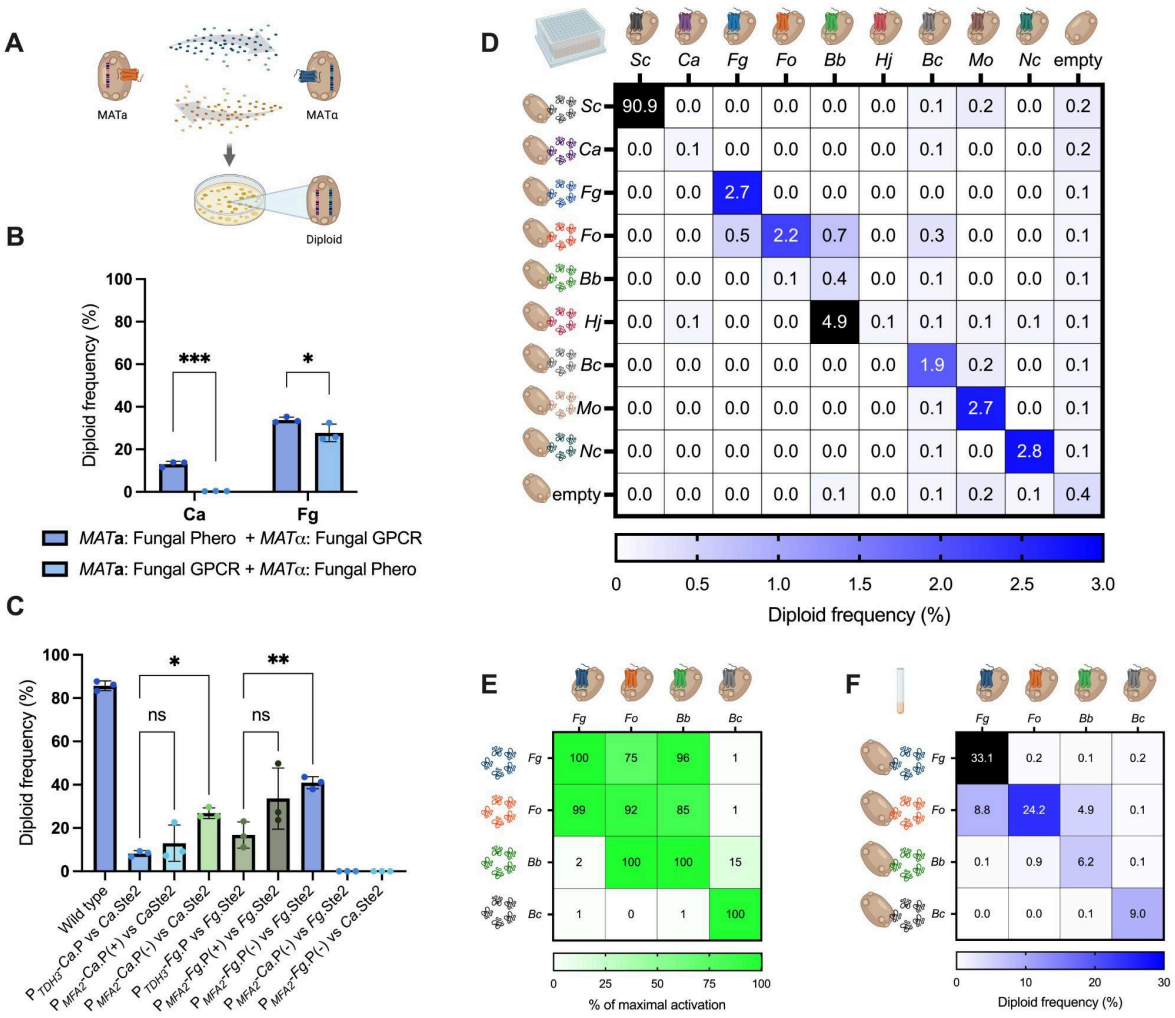

Fig. 1. YeMaP correctly identifies fungal GPCR-pheromone interactions. **A** The One-on-One setting involves co-culturing two strains: the first expresses a heterologous mating receptor and the second secretes a heterologous cognate pheromone. After mating, diploid cells are formed and selected. **B** Comparison in the *Ca* and *Fg* co-cultures was conducted between the following conditions: *MAT***a** cells expressing the fungal pheromone from the *MFA2* promoter (*Ca*: GEN29, *Fg*: GEN35) and *MAT*α cells expressed the fungal GPCR (*Ca*: GEN36, *Fg*: GEN37) against *MAT***a** cells expressing the fungal GPCR (*Ca*: GEN100, *Fg*: GEN78) and *MAT*α cells expressing the fungal pheromone from the *MFα1* promoter (*Ca*: GEN76, *Fg*: GEN77). *MFA2* and *MFα1*

promoters were selected as the strongest inducible pheromone promoters based on previous publications [22,36]. **C** Diploid frequency comparison between different designs. GEN18 and GEN27 were co-cultured as wild-type interactions, from left to right the co-cultured strains were GEN36 co-cultured with GEN28 (P_{TDH3}-Ca.P), GEN29 (P_{MFA2}-Ca.P), or GEN55 (P_{MFA2}-Ca.P, *mfa1*Δ, *mfa2*Δ). GEN37 co-cultured with (P_{TDH3}-Fg.P), GEN35 (P_{MFA2}-Fg.P), or GEN58 (P_{MFA2}-Fg.P, *mfa1*Δ, *mfa2*Δ). Receptors with non-cognate pheromone GEN55 + GEN37 and GEN58 + GEN36. **D** Yeast mating matrix, 10 fungal GPCRs *MAT*α strains (columns) were co-cultured with 10 fungal pheromone *MAT***a** strains (rows). A blue gradient was set to a maximum of 3% of diploid frequency and values above 3% were colored in black. The list of organisms and their pheromones sequence can be found in Supplementary Table 1. **E** Levels of activation of *Fg*.Ste2 (CPK366), *Fo*.Ste2 (GEN70), *Bb*.Ste2 (GEN71) and *Bc*.Ste2 (GEN128) biosensors (columns) incubated with *Fg*, *Fo*, *Bb*, and *Bc* pheromone (rows). Each pheromone was supplemented at a concentration of 10 μM. The fluorescent signal for each GPCR was set to 100% on the highest GFP value (not necessarily with its cognate ligand). **F** Validation of the mating matrix in culture tubes. 4 GPCRs strains GEN37, GEN49, GEN47, GEN48 (columns) were co-cultured with 4 different pheromone strains GEN58, GEN59, GEN56 and GEN57 (rows). A blue gradient was set to a maximum of 30% of diploid frequency and values above 30% were colored in black. Plating was performed in three technical triplicates in **D**, the co-cultures were performed in three biological replicates, and three technical replicates in **B**, **C,** and **F**. Experiments were conducted in four replicates in **E**. Statistical significance was determined in **B** through two-way analysis of variance (ANOVA) with Tukey's multiple comparisons (*$p \leq 0.05$, ***$p \leq 0.0005$) and in **C** with one-way ANOVA with Tukey's multiple comparisons tests in GraphPad Prism (*$p \leq 0.05$, **$p \leq 0.01$).

Screening a library of pheromone variants on a fungal GPCR to identify new pheromone agonists (Library-on-One).

Among the *Sordariomycetes* class, several species with relevant ecological roles in soil have mating pheromones that share a similar backbone[16,37]. As per this natural resemblance, and together with our deciphered interaction network above (Fig. 1F), we narrowed our focus to 4 GPCRs of the three plant pathogens (*Fg*.Ste2, *Fo*.Ste2, and *Bc*.Ste2) and the insect pathogen *Bb* (*Bb*.Ste2) to search for pheromone agonists in a multiplex pool. Our pheromone library (YPL1) was designed to include 262,144 variants (encoding 8,000 pheromone peptides), reaching saturation of three internal residues in the sequence

WCXXXGQPCW (where X is any possible amino acid in position 3, 4, and 5) while preserving the two essential residues Gly6-Gln7, which are responsible for maintaining the three-dimensional structure of the *Fo* pheromone[38]. By adapting a recently established state-of-the-art yeast transformation method[39] we transformed 1.8 x 10^6 yeast cells to get a 6.9x coverage of our library.

We then co-cultured the YPL1 with each single GPCR and sequentially enriched for diploid cells (Fig. 2A). By normalizing the counts in Reads Per Million (RPM) and subtracting the reads of the library before the co-cultures, we observed a specific and exclusive enrichment for the *Bb* pheromone in *Bb*.Ste2 (+307 RPM) and *Fg* pheromone in *Fg*.Ste2 (+807 RPM), however, the *Fo* pheromone was the most enriched sequence for all four receptors included in our screen (>340,000 RPM per sample). To validate the YeMaP results, we performed dose-response curves with chemically synthesized versions of 10 pheromones which were present in the top 20 of the most abundant pheromone sequences in both biological replicates for each GPCR (Supplementary Fig. 3 and Supplementary Table 2). When incubated with the GPCR, for which they were originally enriched, seven out of ten selected pheromones showed strong activation of the pheromone response pathway (Fig. 2B-E). We additionally observed a low activation for two out of the remaining three pheromones (Supplementary Fig. 4A). In the *Bb*.Ste2 biosensor strain, the *Bb* and *Fo* pheromones, which exhibited similar diploid frequencies formation (Fig. 1B), displayed two distinct half-maximal effective concentration (EC_{50}) values (Fig. 2E), with the latter being 4,263-fold higher (*Fo*_EC_{50} = 9.58 x 10^{-7} M compared to Bb_EC_{50} = 2.45 x 10^{-10} M). Similarly to the *Bb* pheromone, the pheromone "Agonist1" (A1) contained a conserved Arg4 residue, preceded by Leu3 and followed by a Pro5, a combination not found in any known organism (Supplementary Fig. 3) but with similar potency to the *Bb* pheromone (A1_EC_{50} = 4.82 x 10^{-10} M).

Our screening assay revealed two pheromones (A4 and A5) for *Fo*.Ste2, both with a conserved Trp4 and at least a 13-fold lower EC_{50} compared to the native pheromone (A4_EC_{50} = 5.16 x 10^{-10} M, A5_EC_{50} = 2.31 x 10^{-9} M, Fo_EC_{50} = 2.92 x 10^{-8} M). We identified

the A5 sequence in the *Fo* α-factor pro sequence (Supplementary Table 5) while A4, which contained an Ala5, was found to be a synthetic pheromone sequence with significantly greater potency, requiring 57 times less pheromone to achieve the same EC_{50} as the native *Fo* pheromone (Fig. 2D).

Molecular dynamic (MD) simulations suggested that all 3 pheromones (*Fo*, A5, and A4) had the same binding pose within the orthosteric pocket of *Fo*.Ste2, in which the carboxylic acid functional group of Trp10 forms salt bridges with Arg84 and Arg187 (Supplementary Fig. 5). We observed that A4 is the most stable from residues 5-10 with special attention to Trp10, which is the anchoring residue to the bottom of the orthosteric binding pocket (Supplementary Fig. 5B).

Next, we asked if our YeMaP dataset could also reliably reveal antagonists. We therefore looked into underrepresented or absent sequences in our analysis. We observed the absence of a pheromone encoded in the *Cordyceps militaris* and *Beauveria asiatica* α-factor pro sequences (Supplementary Table 5) in *Fg*.Ste2, *Fo*.Ste2, *Bc*.Ste2, while its enrichment was observed in *Bb*.Ste2 (+7,508 RPM). We considered this pheromone (named *Cm*) as a potential antagonist that could inhibit diploid formation. *Cm* pheromone showed activation in *Bb*.Ste2 and *Fo*.Ste2, yet no activation in *Fg*.Ste2 or *Bc*.Ste2. When co-incubated with the lowest pheromone concentration capable of inducing GPCR activation, *Cm* pheromone showed an antagonistic action on *Bc*.Ste2 (Supplementary Fig. 4B) and reached a half-maximal inhibitory concentration (IC_{50}) at 1 μM (Fig. 2F). We found a similar effect in *Bc*.Ste2 from co-incubation with the *Bb* pheromone, while no effect was observed with the addition of *Fo* pheromone (Fig. 2G). These two antagonist pheromones (*Cm* and *Bb*) shared eight out of nine residues with *Bc* pheromone. The antagonist effect was only observed when the two residues Arg4 and Pro5 (not present in *Fo* pheromone) were preceded by a Leu^3 or Met^3 instead of Gly3. This feature was combined with the additional Trp10, a residue absent in the nine residues *Bc* pheromone (Supplementary Tables 1-2). The antagonistic effect of the *Cm* pheromone was also apparent in a mating assay. A co-culture consisting of *Bc* GPCR and pheromone strains incubated with 50 μM of *Cm* showed a 2-fold reduction in

diploid formation (p=0.0071) compared to the same co-culture incubated with 50 µM of a scrambled pheromone (Supplementary Fig. 4D).

In conclusion, by conducting a straightforward "Library-on-One" assay using YeMaP, we could retrieve agonists and one antagonist by choosing either the most or least enriched sequences, respectively, for simple validation assays.

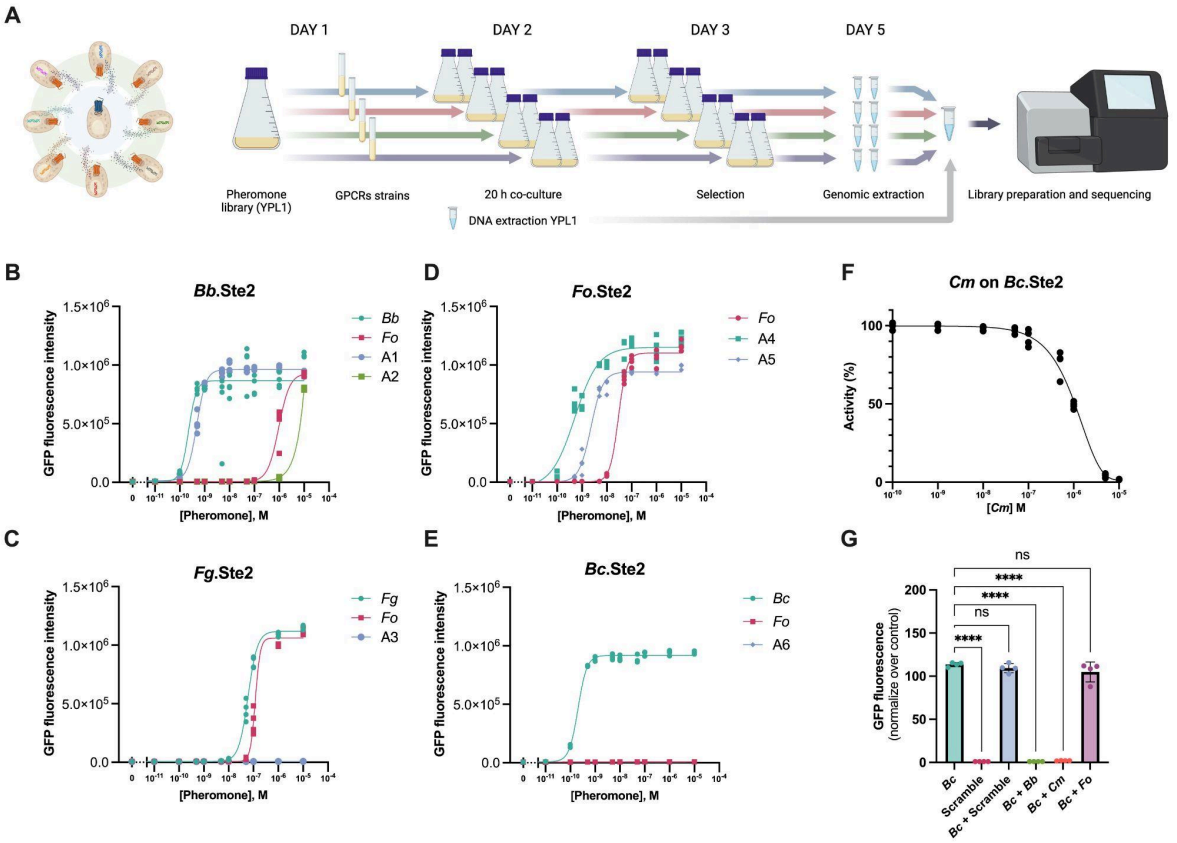

Fig. 2. Detection of agonists and an antagonist from a library of pheromone variants. A After the generation of YPL1, the library was co-cultured with *Bb*.Ste2 (GEN88), *Fg*.Ste2 (GEN87), *Fo*.Ste2 (GEN90) or *Bc*.Ste2 (GEN89) for 20 h in 8 different shake flasks (2 per mating receptor). After 2 days of enrichment, gDNA was extracted and used for sequencing on NextSeq 500. Results of the dose-response curves, the most enriched pheromones in **B** *Bb*.Ste2 (*Fo*, A1 and A2), **C** *Fg*.Ste2 (*Fo* and A3), **D** *Fo*.Ste2 (*Fo*, A4, and A5) and **E** *Bc*.Ste2 (*Fo* and A6) were compared with the cognate pheromone of each receptor (*Bb*, *Fg*, *Fo*, and *Bc*). **F** inhibition curve of *Bc*.Ste2 (GEN128) co-cultured with 0.0005 µM of *Bc* pheromone and an increased amount of *Cm* pheromone. **G** Fold change activation of *Bc*.Ste2 (GEN128) over control with 0.0005 µM of *Bc* pheromone (positive control), 10 µM of Scramble peptide (negative control), and different combinations of *Bc* and 10 µM of Scramble, *Bb*, *Cm* and *Fo* pheromone. The combination *Bc* + Scramble and *Bc* + *Fo* didn't differ from the

condition with *Bc* pheromone. The activation was completely abolished when *Bc* or *Cm* pheromones were present. Means represents four biological replicates. Statistical significance was determined using one-way ANOVA with Dunnett's multiple comparison test in GraphPad Prism (****$p < 0.0001$).

Abiotic factors shape the interaction networks between multiple fungal components (Library-on-Library).

In order to study multiple network interactions simultaneously, and to understand the influence of abiotic factors on fungal cell-cell communication networks, we introduced a barcode system based on Cre-lox recombinase[40]. In brief, each haploid cell contained a conserved region flanked by a barcode of 20 bp, a spacer, and a Lox site (Table 5). After successful mating, a unidirectional recombination event positions the two barcodes on the same chromosome[20] (Fig. 3A). Using quantitative PCR (qPCR) to link two barcodes and the association between a pheromone and a GPCR, we could estimate the relative abundances of diploid cell types in a pool. The relative abundance of a diploid was compared with the abundance of all diploids containing the conserved regions (R1 + R3) flanking the two barcodes (see Methods section). We first tested the specificity of the system by running 4 different co-cultures and combinations of these co-cultures in consortia, assessing that the two barcode sites were on the same chromosome (Supplementary Fig. 6). Notably, the empty constructs (no_Pheromone and no_GPCR) were capable of forming diploids in a co-culture (Fig. 1D and Supplementary Fig. 6) but their presence was not detected in consortia with other strains (Supplementary Fig. 6). The introduction of barcodes in the remaining strains brought specific amplification and detection of diploids using qPCR. From all co-cultures tested, the relative diploid abundance detected with each set of primers was comparable (Supplementary Fig. 7 and Supplementary Data 3).

To mimic the presence of multiple fungal organisms of ecological interest, we performed consortia with *Fg*, *Fo*, *Hj*, *Bb* GPCRs, and pheromone strains by adding two negative controls (empty strains). We combined these 10 different strains into pre-culture tubes with four different abiotic factors, three different pH (Unbuffered, pH=6, and pH=7), and the

addition of Horse Radish Peroxidase (pH=6 + HRP) to mimic a plant root environment[12]. Interestingly, the *Fo* communication system was the most robust and consequently more effective in the formation of diploid cells in all the conditions tested (Fig. 3B-E). Conversely, in the *Fg* system, which had the second most abundant diploid formation in unbuffered media, media pH=6, and pH=7, the addition of HRP significantly reduced the formation of diploid cells containing *Fg*.Ste2 and pheromone (p=0.023, Supplementary Fig. 8A). In the case of the *Bb* and *Hj* systems, we observed a similar trend: the media at pH=7 led to decreased relative abundance of diploid cells (*Bb* p=0.013, *Hj* p=0.025), and a reduction of their formation was observed when HRP was present in the media at pH=6 (*Bb* p=0.020 *Hj* p=0.021, Supplementary Fig. 8A). Once again we compared the results from the yeast mating platform to our biosensor strains. We only observed activation of the background strain with no mating receptor in Synthetic Complete (SC) unbuffered media with 2 μM HRP and a general activation trend (≈1.5 fold increase in GFP fluorescence) at pH=6 + 2 μM HRP in the background strain and all the biosensors tested (Supplementary Fig. 9A-B).

To elucidate the effect of HRP on each cell-cell communication system, we performed co-cultures of the *Fg*, *Fo*, *Bb*, and *Hj* GPCR-pheromone pairs in the four conditions above and selected the resulting diploid cells on agar plates. As expected we observed a decline in the diploid formation with increasing pH and the presence of HRP in all co-cultures, except for the *Fo* mating pair which showed no reduction but instead a significant rise in diploid formation when HRP was present (p=0.023, Supplementary Fig. 8B).

Taken together, our results demonstrate a synthetic system to study simultaneously how abiotic factors influence the cell-cell communication between different fungal GPCRs and pheromones.

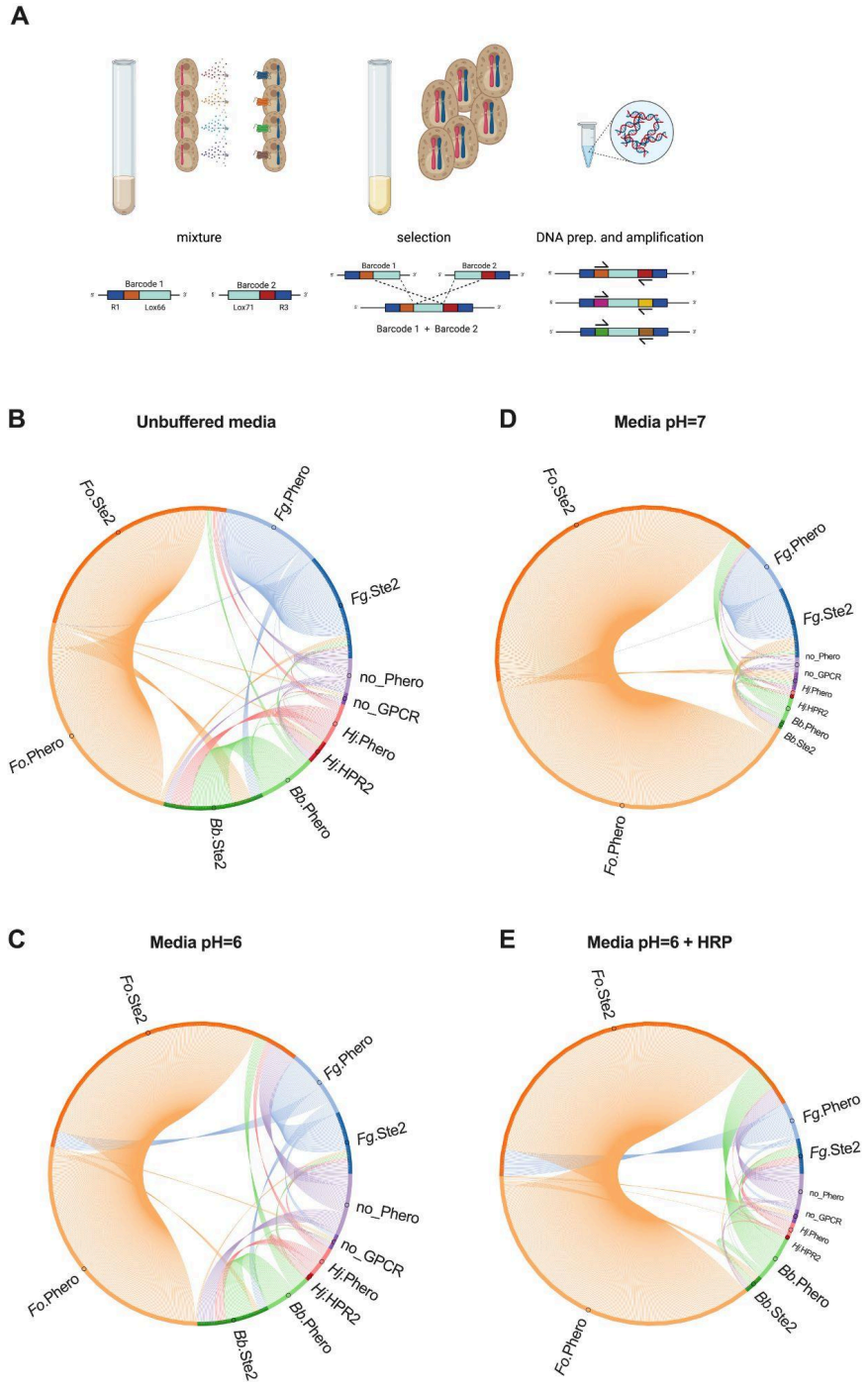

Fig. 3. Abiotic factors govern fungal cell-cell communication A schematic illustration of the barcode system, both *MAT***a** and *MAT*α cells contain a barcode flanked by a conserved region and a Cre-Lox recombination site on chromosome X. After successful mating the two barcodes can recombine and move on the same chromosome. **B-E** Chord diagrams of the 5x5 consortia in **B** Unbuffered media (pH=5.6), **C** a buffered media at

pH=6, **D** buffered media pH=7 and **E** buffered media at pH=6 with 1 μM of Horse Radish peroxidase (HRP). A darker color represents the GPCR strain while the lighter version represents the cognate pheromone strain. Orange=*Fo*, Blue=*Fg*, Green=*Bb*, Red=*Hj*, Violet=control with empty constructs. Every arc represents the connection between a GPCR and a pheromone strain. The size of an arc reflects the relative abundance of a diploid cell. The relative quantification was done by comparing the cycle threshold (Ct) value of every possible combination of two barcodes with the Ct value of the conserved region flanking all barcodes. Every experiment was conducted in three biological replicates.

Pheromone supplementation alters the cell-cell communication of pathogens in a consortium.

After assessing the influence of abiotic factors on four different fungal GPCR-pheromone pairs and showing the robustness of *Fo* components, we combined all the knowledge acquired to this point with YeMaP. With the intention to limit the plant pathogens (*Fo* and *Fg*)[41] and promote the non-pathogenic/commensal (*Bb* or *Hj*) cell-cell communication[42,43], we investigated the effect of the scrambled, *Cm*, and A4 pheromone supplementations. As shown in **Fig. 4**, almost every diploid found in SC media was formed based on the *Fo*.Ste2 + *Fo*.Pheromone or *Fg*.Ste2 + *Fg*.Pheromone pairs (Fig. 4A). The same situation was observed in SC media + 10 μM of a scrambled peptide (Fig. 4B). A different scenario was observed for *Cm* or A4 pheromone supplementations (Fig. 4C-D): In the first case, we observed 0.2-fold decline in diploids containing *Fo*.Ste2 (p=0.001) and 2.2-fold increase in diploids containing *Fg*.Ste2 (p=0.015). In the second case, we noticed 8.7-fold and 12.1-fold increased formation of diploids containing *Bb*.Ste2 (p=0.004) and *Hj*.HPR2, respectively (p=0.001), yet in conjunction with a 19-fold increase in the negative control without a GPCR (p=0.013). A4 pheromone supplementations reduced the presence of diploid with *Fo*.Ste2 by 0.2-fold (p=0.001), without increasing the presence of diploids containing *Fg*.Ste2. *Fg*.Ste2 and *Fg*.Pheromone interaction was reduced by 0.3-fold, however, *Fo*.Pheromone strain

compensated for the final amount of diploids containing the *Fg*.Ste2 (Supplementary Fig. 10A).

Furthermore, media with different nitrogen sources, which are also common fertilizers, exhibited distinct distributions of the relative diploid abundances. Compared to SC media with ammonium sulfate (SC), SC media with ammonium sulfate and Urea (SC-AS/Urea) had a 4-fold and 20-fold increase of diploids containing *Bb*.Ste2 and *Hj*.HPR2, respectively (Supplementary Fig. 10B). The nitrogen source did not affect the abundance of diploids with *Fo*.Ste2, and the control strain with no_GPCR while SC-AS/Urea decreased 0.8-fold the abundance of diploids with *Fg*.Ste2 (Supplementary Fig. 10B).

In summary, through YeMaP, we could reconstruct a network of interactions between fungal GPCRs and pheromones in which we could subsequently control the cell-cell communication mediated by GPCRs of pathogenic origins.

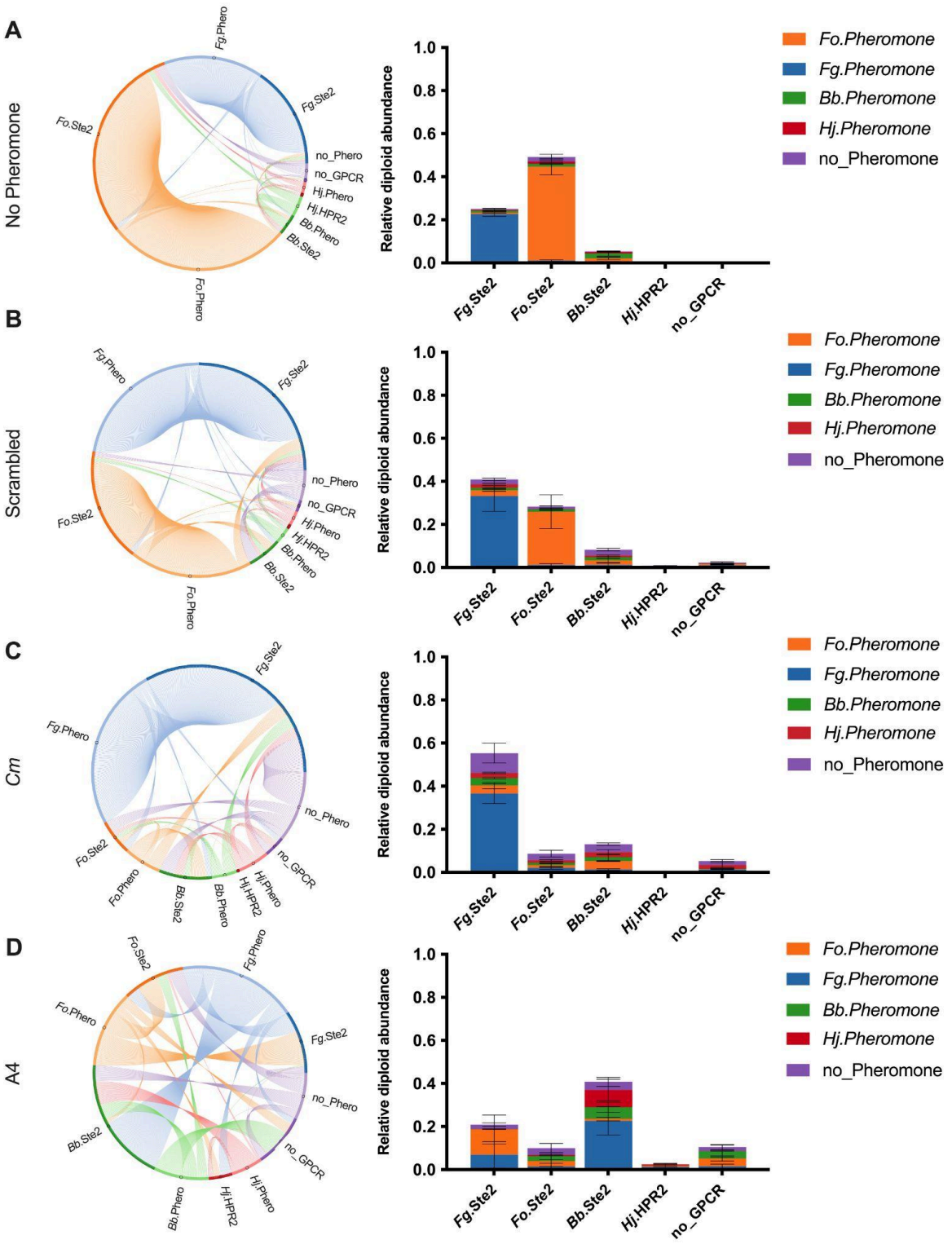

Fig. 4. Cell-cell communication in a consortium can be shaped by pheromone supplementation. Starting from SC media without any supplementation of pheromone in **A**, we performed consortia with **B** SC with 10 μM of Scramble peptide (negative control), **C** SC with 10 μM of *Cm* pheromone, and **D** SC with 10 μM of A4 pheromone. On the left, in the chord diagrams a darker color represents the GPCR strain while the lighter version

represents the cognate pheromone strain. Orange=*Fo*, Blue=*Fg*, Green=*Bb*, Red=*Hj*, Violet=control with empty constructs. Every arc represents the connection between a GPCR and a pheromone strain. The size of an arc reflects the relative abundance of a diploid cell. The relative quantification was done by comparing the Ct value of every possible combination of two barcodes with the Ct value of the conserved region flanking all barcodes. On the right, the bar plots represent the distribution of pheromone strains that have successfully mated with the five GPCR strains. Every experiment was conducted in three biological replicates.

Discussion

Fungal hyphae can sense a variety of chemical cues and grow toward nutrient sources, mating partners, or host organisms[44]. Here we have established a yeast mating platform (YeMaP) to decipher fungal GPCR-pheromone interactions and investigate how these interactions are affected by abiotic factors or can be controlled through pheromone supplementations. YeMaP displayed increased resolution compared to the standard designs for yeast biosensors[14,45,46] (Fig 1C-D), these differences may be explained by the well-documented role of the Sst2 protein in suppressing signaling noise and GPCR activation[47–49]. Accordingly, GPCR signaling did not always translate to a comparable mating efficiency. For example, from the pheromone library screen (see Library-on-One) one of the most enriched pheromones (A4) and one of the least enriched pheromones (*Cm*) for *Fo*.Ste2 resulted in being agonists for *Fo*.Ste2 (Fig. 2D and Supplementary Fig. 4C) and consequently affected *Fo*.Ste2 activity in Library-on-Library interaction networks (Fig. 4C-D).

YeMaP already generated new insights into fungal cell-cell communication:

i) The apparent robustness of *Fo*.Ste2 and *Fo* pheromone interaction compared to the *Fg*, *Bb*, and *Hj* cell-cell communication. This result aligns well with the essential role of these components in spore germination[11] and the regulation of Fusaric acid production[50].

ii) The promiscuity of *Bb*.Ste2 particularly towards the *Fo* pheromone. Several reports have described the role of *Bb* in controlling *Fo* virulence for increasing tomato plants' survival rate[51,52], and our results indicate that *Bb* can detect *Fo* pheromone which may define a metabolic program in response to it (Supplementary Fig. 2A).

iii) We observed a general mechanism of activation of the pheromone response pathway in yeast biosensors with HRP supplementation (Supplementary Fig. 8A-B). However, HRP supplementation had different outcomes on YeMaP, such as destabilizing the *Fg*, *Hj*, and *Bb* communication systems, without affecting *Fo*.Ste2 and *Fo* pheromone interaction (Supplementary Fig. 9). Although *Fo* and *Fg* can sense plant roots[12] or exudates[53], our data suggest that their mechanisms have evolved differently. In the presence of HRP, *Fo* was able to maintain the GPCR-pheromone communication, while *Fg* lost it.

We successfully screened a library of 8,000 pheromone variants and detected the *Fo* pheromone as the most enriched for the 4 GPCRs tested. Even though we observed enrichment for the cognate pheromones, the presence of a mixture of different pheromones and synthetic sequences could have played a role in advantaging those with higher EC_{50} values (*Fo*, A1, and A2 in *Bb*.Ste2 and *Fo* in *Fg*.Ste2) or almost no effect such as A3 in *Fg*.Ste2 (Fig. 2 and Supplementary Fig. 4A).

A different outcome was observed for *Fo*.Ste2, with the enrichment of two pheromones with lower EC_{50} values and higher potencies, further highlighting this communication system's different behavior. For the *Bc*.Ste2, a mating receptor that has evolved to sense a pheromone with 9 residues instead of 10, we have shown the antagonist effect of fungal pheromones (*Cm* and *Bb*) belonging to different organisms (Fig. 2F-G) and presented a new hypothesis stating that antagonistic pheromones exist and can be used for partner discrimination and chemotropism inhibition in fungi (Supplementary Fig. 4D).

Nevertheless, YeMaP captured the complexity of multiple GPCR-pheromone interactions in the library-on-library sections and exploited them with pheromone supplementations to promote the communication of non-plant pathogenic fungal GPCRs. In the future, we envision using YeMaP as a model for studying how different soil compositions and fertilizers influence cell-cell communication within fungal consortia, and for developing new ways to control fungal pathogen virulence by perturbing their natural ability to engage in cell-cell communication.

Acknowledgements

This study is supported by grants from the Villum Foundation (00050095) to L.C. and M.K.J., Novo Nordisk Foundation NNF20CC0035580 (core grant) to M.K.J., E.D.J., V.K., E.Ö., and P.C.M, the Wenner-Gren Foundation to M.W, Novo Nordisk Foundation NNF23SA0084103 to T.M.F., and the Bioscience Ph.D. Program to R. T. (NNF0078230).

We thank Dr. Alvaro De Obeso-Fernández del Valle, Dr. José Mario González-Meljem, and Kinga Dulak for their technical support on the plating and the creation of the One-on-One matrix. We thank Keyan Liu for the technical support on the Illumina sequencing and Philip Tinggaard Thomsen for providing the plasmid pCfB10291. We thank Sara Lestani for the scientific discussion.

Author contributions

GS, EDJ, LC, and MKJ conceived the study. GS led the investigation. GS designed and constructed all yeast strains and plasmids of this study. GS and AU performed the *B. bassiana* experiments. AU and DR performed the LC-MS. AU conducted the targeted metabolome analysis, and MBS performed the metabolome untargeted data analysis. GS and MW generated the yeast pheromone library, while GS and MJ conducted the data analysis of the Illumina libraries. RT performed the Molecular Dynamics simulations. EEHS and MD supported the investigation. GS conducted all the remaining experiments and data analysis. GS, EDJ, and MKJ wrote the manuscript. MKJ, LC, TMF, PCM, EÖ, VK, MW, and EDJ acquired the funding to enable this research. All authors approved the manuscript.

References

1. Taylor, D. L. & Bhatnagar, J. M. Chapter 4 - Fungi in soil: a rich community with diverse functions. in *Soil Microbiology, Ecology and Biochemistry (Fifth Edition)* (eds. Paul, E. A. & Frey, S. D.) 75–129 (Elsevier, 2024).
2. World Health Organization. *WHO Fungal Priority Pathogens List to Guide Research, Development and Public Health Action*. (World Health Organization, 2022).
3. Stukenbrock, E. & Gurr, S. Address the growing urgency of fungal disease in crops. *Nature* **617**, 31–34 (2023).
4. Singh, B. K. *et al.* Climate change impacts on plant pathogens, food security and paths forward. *Nat. Rev. Microbiol.* **21**, 640–656 (2023).
5. Xue, C., Hsueh, Y.-P. & Heitman, J. Magnificent seven: roles of G protein-coupled receptors in extracellular sensing in fungi. *FEMS Microbiol. Rev.* **32**, 1010–1032 (2008).
6. Brown, N. A., Schrevens, S., van Dijck, P. & Goldman, G. H. Fungal G-protein-coupled receptors: mediators of pathogenesis and targets for disease control. *Nat Microbiol* **3**, 402–414 (2018).
7. Velazhahan, V., McCann, B. L., Bignell, E. & Tate, C. G. Developing novel antifungals: lessons from G protein-coupled receptors. *Trends Pharmacol. Sci.* **44**, 162–174 (2023).
8. Surendra K, D. The new integrated pest management paradigm for the modern age. *J. Integr. Pest Manag.* **10**, (2019).
9. Bardwell, L. A walk-through of the yeast mating pheromone response pathway. *Peptides* **26**, 339–350 (2005).
10. Sieber, B., Coronas-Serna, J. M. & Martin, S. G. A focus on yeast mating: From pheromone signaling to cell-cell fusion. *Semin. Cell Dev. Biol.* **133**, 83–95 (2023).
11. Vitale, S., Di Pietro, A. & Turrà, D. Autocrine pheromone signalling regulates community behaviour in the fungal pathogen Fusarium oxysporum. *Nat Microbiol* **4**, 1443–1449 (2019).
12. Turrà, D., El Ghalid, M., Rossi, F. & Di Pietro, A. Fungal pathogen uses sex pheromone

receptor for chemotropic sensing of host plant signals. *Nature* **527**, 521–524 (2015).

13. Sridhar, P. S. *et al.* Ste2 receptor-mediated chemotropism of Fusarium graminearum contributes to its pathogenicity against wheat. *Sci. Rep.* **10**, 10770 (2020).
14. Ostrov, N. *et al.* A modular yeast biosensor for low-cost point-of-care pathogen detection. *Sci Adv* **3**, e1603221 (2017).
15. Billerbeck, S. *et al.* A scalable peptide-GPCR language for engineering multicellular communication. *Nat. Commun.* **9**, 5057 (2018).
16. Martin, S. H., Wingfield, B. D., Wingfield, M. J. & Steenkamp, E. T. Causes and consequences of variability in peptide mating pheromones of ascomycete fungi. *Mol. Biol. Evol.* **28**, 1987–2003 (2011).
17. Vangalis, V. *et al.* Components of TOR and MAP kinase signaling control chemotropism and pathogenicity in the fungal pathogen Verticillium dahliae. *Microbiol. Res.* **271**, 127361 (2023).
18. Lengger, B. & Jensen, M. K. Engineering G protein-coupled receptor signalling in yeast for biotechnological and medical purposes. *FEMS Yeast Res.* **20**, (2020).
19. Yashiroda, Y. & Yoshida, M. Intraspecies cell-cell communication in yeast. *FEMS Yeast Res.* **19**, (2019).
20. Younger, D., Berger, S., Baker, D. & Klavins, E. High-throughput characterization of protein–protein interactions by reprogramming yeast mating. *Proceedings of the National Academy of Sciences* **114**, 12166–12171 (2017).
21. Angermueller, C. *et al.* High-throughput ML-guided design of diverse single-domain antibodies against SARS-CoV-2. *bioRxiv* 2023.12.01.569227 (2023) doi:10.1101/2023.12.01.569227.
22. Jensen, E. D. *et al.* Engineered cell differentiation and sexual reproduction in probiotic and mating yeasts. *Nat. Commun.* **13**, 6201 (2022).
23. Janiak, A. M. *et al.* Functional expression of the Candida albicans α-factor receptor in Saccharomyces cerevisiae. *Fungal Genet. Biol.* **42**, 328–338 (2005).
24. Gonçalves-Sá, J. & Murray, A. Asymmetry in sexual pheromones is not required for

ascomycete mating. *Curr. Biol.* **21**, 1337–1346 (2011).

25. Anders, A., Colin, R., Banderas, A. & Sourjik, V. Asymmetric mating behavior of isogamous budding yeast. *Sci. Adv.* **7**, eabf8404 (2021).
26. Huberman, L. B. & Murray, A. W. Genetically engineered transvestites reveal novel mating genes in budding yeast. *Genetics* **195**, 1277–1290 (2013).
27. Michaelis, S. & Barrowman, J. Biogenesis of the Saccharomyces cerevisiae pheromone a-factor, from yeast mating to human disease. *Microbiol. Mol. Biol. Rev.* **76**, 626–651 (2012).
28. McAlister, L. & Holland, M. J. Differential expression of the three yeast glyceraldehyde-3-phosphate dehydrogenase genes. *J. Biol. Chem.* **260**, 15019–15027 (1985).
29. Nishi, O., Sushida, H., Higashi, Y. & Iida, Y. Epiphytic and endophytic colonisation of tomato plants by the entomopathogenic fungus Beauveria bassiana strain GHA. *Mycology* **12**, 39–47 (2020).
30. Gupta, R. *et al.* The entomopathogenic fungi Metarhizium brunneum and Beauveria bassiana promote systemic immunity and confer resistance to a broad range of pests and pathogens in tomato. *Phytopathology* **112**, 784–793 (2022).
31. Wang, X., Gong, X., Li, P., Lai, D. & Zhou, L. Structural diversity and biological activities of cyclic depsipeptides from fungi. *Molecules* **23**, (2018).
32. Amobonye, A., Bhagwat, P., Pandey, A., Singh, S. & Pillai, S. Biotechnological potential of Beauveria bassiana as a source of novel biocatalysts and metabolites. *Crit. Rev. Biotechnol.* **40**, 1019–1034 (2020).
33. Smilde, A. K. *et al.* ANOVA-simultaneous component analysis (ASCA): a new tool for analyzing designed metabolomics data. *Bioinformatics* **21**, 3043–3048 (2005).
34. Schmid, R. *et al.* Integrative analysis of multimodal mass spectrometry data in MZmine 3. *Nat. Biotechnol.* **41**, 447–449 (2023).
35. Nothias, L.-F. *et al.* Feature-based molecular networking in the GNPS analysis environment. *Nat. Methods* **17**, 905–908 (2020).

36. Jacobs, K. C., Gorman, O. & Lew, D. J. Mechanism of commitment to a mating partner in *Saccharomyces cerevisiae*. *Mol. Biol. Cell* **33**, (2022).
37. Le Marquer, M., San Clemente, H., Roux, C., Savelli, B. & Frei Dit Frey, N. Identification of new signalling peptides through a genome-wide survey of 250 fungal secretomes. *BMC Genomics* **20**, 64 (2019).
38. Vitale, S. *et al.* Structure-activity relationship of α mating pheromone from the fungal pathogen Fusarium oxysporum. *J. Biol. Chem.* **292**, 3591–3602 (2017).
39. Wäneskog, M. *et al.* Heat pre-treatment reduces multiplicity of plasmid transformations in yeast during electroporation, without diminishing the transformation efficiency. *bioRxiv* 2024.07.03.601847 (2024) doi:10.1101/2024.07.03.601847.
40. Araki, K., Araki, M. & Yamamura, K.-I. Site-directed integration of the cre gene mediated by Cre recombinase using a combination of mutant lox sites. *Nucleic Acids Res.* **30**, e103 (2002).
41. Dean, R. *et al.* The Top 10 fungal pathogens in molecular plant pathology. *Mol. Plant Pathol.* **13**, 414–430 (2012).
42. Schmoll, M. Trichoderma reesei. *Trends Microbiol.* **30**, 403–404 (2022).
43. Ownley, B. H. *et al.* Beauveria bassiana: endophytic colonization and plant disease control. *J. Invertebr. Pathol.* **98**, 267–270 (2008).
44. Brand, A. & Gow, N. A. R. Mechanisms of hypha orientation of fungi. *Curr. Opin. Microbiol.* **12**, 350–357 (2009).
45. Shaw, W. M. *et al.* Engineering a model cell for rational tuning of GPCR signaling. *Cell* **177**, 782–796.e27 (2019).
46. Crnković, T., Bokor, B. J., Lockwood, M. E. & Cornish, V. W. Peptide Variant Detection by a Living Yeast Biosensor via an Epitope-Selective Protease. *BioDesign Res* **5**, (2023).
47. Dixit, G., Kelley, J. B., Houser, J. R., Elston, T. C. & Dohlman, H. G. Cellular noise suppression by the regulator of G protein signaling Sst2. *Mol. Cell* **55**, 85–96 (2014).
48. Dohlman, H. G., Song, J., Ma, D., Courchesne, W. E. & Thorner, J. Sst2, a negative

regulator of pheromone signaling in the yeast Saccharomyces cerevisiae: expression, localization, and genetic interaction and physical association with Gpa1 (the G-protein alpha subunit). *Mol. Cell. Biol.* **16**, 5194–5209 (1996).

49. Bush, A. *et al.* Yeast GPCR signaling reflects the fraction of occupied receptors, not the number. *Mol. Syst. Biol.* **12**, 898 (2016).
50. Staropoli, A. *et al.* Repression of autocrine pheromone signaling leads to fusaric acid over-production. *Nat. Prod. Res.* **38**, 1967–1971 (2024).
51. Nchu, F. *et al.* Endophytic Beauveria bassiana induces oxidative stress and enhances the growth of Fusarium oxysporum-infected tomato plants. *Plants* **11**, 3182 (2022).
52. Ranesi, M. *et al.* Field isolates of Beauveria bassiana exhibit biological heterogeneity in multitrophic interactions of agricultural importance. *Microbiol. Res.* **286**, 127819 (2024).
53. Sridhar, P. S., Vasquez, V., Monteil-Rivera, F., Allingham, J. S. & Loewen, M. C. A peroxidase-derived ligand that induces Fusarium graminearum Ste2 receptor-dependent chemotropism. *Front. Cell. Infect. Microbiol.* **13**, 1287418 (2023).

Methods

Molecular cloning for yeast engineering

Gene blocks and DNA parts

Gene blocks gDOG1 to gDOG10 were codon optimized for *Saccharomyces cerevisiae* with the IDT Codon Optimization tool. All oligos and gene blocks were purchased from IDT, and coding sequences were immediately preceded by a transcriptional enhancer sequence (AAAACA).

PCR and DNA handling

Plasmids were assembled with USER cloning [1] to be compatible with the EasyClone-MarkerFree system for CRISPR/Cas9 engineering [2] and adapted to the MAD-cloning strategy [3]. All strains, plasmids, oligos, gBlocks, and parts are listed in the Supplementary Data 1.

Bacterial handling for plasmid construction and propagation

Plasmids were transformed (heat-shocked) in *E.coli* DH5α strain. The competent cells were stored in glycerol at -70°C and cultivated in Terrific Broth with ampicillin (100 mg/L) at 37°C in liquid media at 300 r.p.m. or on agar plates for 16-20 hrs.

Strains, media, and transformation

Strains

Beauveria bassiana (DSM 62075) strain was obtained from the Leibniz Institute DSMZ-German Collection of Microorganisms and Cell Cultures. Strain CEN.PK2-1C and BY4741 (EUROSCARF) were used as yeast background strains.

Media

Yeast strains were grown in Synthetic Complete (SC) media with 2% (w/v) glucose with a pH=5.6 or in a buffered media with ammonium sulfate, urea, and the citrate phosphate buffer system (0.1 x) following Prins et al. protocol [4]. *B. bassiana* was grown on YPD plates with 2% (w/v) glucose and supplementation on top of the plate of 100 µl of MeOH (50% v/v), *Bb*, *Fo*, or a scrambled version of *Fo* pheromone (378 µM).

Transformation

Except for the Yeast pheromone library (YPL1, see below), all strains were generated using the LiAc/ssDNA/PEG method [5]. All genetic cassettes were integrated into the genome of strains harboring pEDJ391 to express CRISPR-Cas9 [6]. Genomic integration was achieved with the co-transformation of a *NotI* linearized fragment with homology arms and a gRNA helper vector targeting the desired EasyClone site [2]. About 1–2 µg for each plasmid or fragment of DNA was used in all chemical transformations of *S. cerevisiae*. The strain was selected in SC with 2% (w/v) glucose media lacking the appropriate amino acid or with the addition of 100 mg/L nourseothricin (Jena Bioscience, Cat.#AB-101).

Yeast Pheromone Library (YPL1)

YPL1 was generated by PCR amplifying two fragments F1 (of 1978 bp generated with XI-3 UP FW + DOG105) and F2 (of 961 bp generated with DOG106 + XI-3 RV) with 129 bp of homology between each other. The plasmid pDOG44 was used as a template (Supplementary Table 4). Electroporation was conducted as described by Wäneskog et al. [7] with few modifications. The strain GEN74 was streaked on a SC-leu plate. A colony was

inoculated in 60 ml of YPD and incubated at 30°C with vigorous aeration for 24 h. 40 mL of the stationary yeast culture was added to 400 ml (1/10 dilution) of fresh YPD and incubated for 3h at 30°C with vigorous aeration. 400 ml of the yeast culture were centrifuged at 4000xg for 5 minutes by first aliquoting the yeast culture in 8 falcon tubes. The YPD supernatant was discarded, and the yeast cell pellets were pooled into 1 falcon by resuspending them in a total of 50ml pre-chilled (4°C) Milli-Q H_2O twice. The yeast cells were pelleted by centrifugation at 4000xg for 5 minutes before resuspending in 50 ml of a 1M sorbitol and 1 mM $CaCl_2$ solution. The osmotically shocked yeast cells were pelleted at 4000xg for 5 minutes, and the yeast cells were resuspended in 50 ml of a 100 mM Lithium Acetate (LiAc) and 10 mM Dithiothreitol (DTT) solution. The cells in LiAc and DTT solution were incubated at 30°C with vigorous aeration for 1h, pelleted at 4000xg for 5 minutes, resuspended in 50 ml of a 1 M sorbitol and 1 mM $CaCl_2$ solution, followed by another final pelleting at 4000xg for 5 minutes. The volume of the yeast cell solution was then adjusted to the total volume of 4ml, by adding the necessary volume of a 1 M sorbitol and 1 mM $CaCl_2$ solution. An aliquot of the yeast solution is removed, and serial diluted by a 10-fold serial dilution. 100 µl of this diluted cell solution from dilutions 10^{-5} and 10^{-6} was plated on a YPD 2% (w/v) agar plate that was then incubated at 30°C for 48 hours before the concentration of cells (CFU/ml) in the transformation solution was enumerated via colony count. 400 µl of the yeast solution was used per transformation reaction by mixing the cell suspension with 5 mg of plasmid DNA (or any other DNA to be transformed), 5 mg of F1, 5 mg of F2, 5 mg of pESC_URA_gRNA_XI-3 plasmid and 10µl (100µg) of boiled single-stranded salmon sperm carrier DNA (ssDNA) in an Eppendorf tube. The yeast, DNA, and ssDNA mix were then transferred to an electroporation cuvette (2mm gap), and the solution was electroporated at 2.0 kV, 200 Ohm, and 25µFD. Surviving cells and transformed cells were enumerated by serial diluting the recovered cell suspension and then plating each dilution on YPD (surviving cells) or SC -leu -ura (transformed cells). The library was expanded in SC -leu -ura for 48 hours and aliquots were stored in glycerol stock at -70°C. We avoid the introduction of a second pheromone

sequence in the diploid cells, due to the potential presence of the Cas9 and gRNA plasmids, by introducing a mutation in the XI-3 site of the biosensor strains.

Experimental procedures

Mating trials

One-on-One in a tube. MATa and MATα strains were inoculated from a cryo stock into a culture tube with 1 ml of SC -leu and SC -his respectively (30 °C, 250 RPM, overnight). Reaching a final OD=0.1 with a 1:1 ratio around 5 µl from a saturated MATa culture and 5 µl from a saturated MATα culture were combined into a culture tube with 1 ml of SC media and for 20 hours (30 °C, 250 RPM). The haploids were plated in SC -leu (MATa strains) and SC -his (MATα strains) in 3 plates per strain. After 20 hours the diploid cells were appropriately diluted and plated in SC -leu -his plates. The colonies on plates were enumerated after 4 days of incubation at 30 °C using the Count This app installed on an iPhone.

One-on-One in a deep well plate. Similarly to the One-on-One in tube assay 2 µl from a saturated MATa culture and 2 µl from a saturated MATα culture were combined into 250 ml of SC media and incubated at 30 °C in a shaking incubator for 20 hours (30 °C, 250 RPM). Enumeration of haploid and diploid cells was conducted in the same way.

Library-on-One- GPCR against the yeast pheromone library. Two full cryotubes of the yeast pheromone library (YPL1) were inoculated into a flask containing 50 ml of SC -leu. GEN87 (*Fg*.Ste2), GEN88 (*Bb*.Ste2), GEN89 (*Bc*.Ste2), and GEN90 (*Fo*.Ste2) were inoculated from the cryostock in 4 different tubes containing 4 ml of SC -his (30 °C, 250 RPM). YPL1 was co-cultured with each single receptor in a shake flask with 50 ml of SC in two biological replicates with a final OD=0.2 and a ratio of MATa 1:1 MATα. After 20 hours 1 ml of the co-culture was washed twice with Milli-Q water and transferred into a flask with 50 ml of SC

-his -leu (30 °C, 250 RPM). The culture was left growing for 48 hours (30 °C, 250 RPM) and 5 ml of it was used to perform a genome extraction using the yeast DNA extraction kit (ThermoFisher).

Library-on-Library - poly-cultures with pheromones and GPCRs. MATa and MATα strains were inoculated from a cryo stock into culture tubes with 1 ml of SC -leu and SC -his respectively (30 °C, 250 RPM, overnight). All MATa and MATα strains were mixed in two different tubes by adding the same amount of volume from the starting tubes. 50 µl of MATa and 50 µl of MATα were combined in culture to reach a final volume of 5 ml and incubated at 30 °C in a shaking incubator for 20 hours (30 °C, 250 RPM). Genomic DNA was extracted from all cultures using the Yeast DNA extraction kit (ThermoFisher).

qPCR protocol

From the *Library-on-Library* experiments, 50 ng of genomic DNA was used as a template to detect the relative abundance of diploid formation. Each condition was tested in 3 biological replicates. All qPCR reactions were performed using SYBR Master Mix (ThermoFisher) on the QuantStudio 5 system.

Handling of synthetic pheromones

Synthetic peptides (Supplementary Table 2) were purchased by GenScript Biotech (4 mg, ≥95% purity) and dissolved in 100% DMSO to a concentration of 1000 µM, then tenfold diluted in SC media to 1000 µM (10% DMSO). A serial dilution in SC + 10% DMSO was made to achieve a concentration of 1×10^{-11}, 1×10^{-10}, 5×10^{-10}, 1×10^{-9}, 5×10^{-9}, 1×10^{-8}, 5×10^{-8}, 1×10^{-7}, 1×10^{-6}, 1×10^{-5} M for the dose-response curve. For the *B. bassiana* chemotropism assay and growth on YPD plates, *Bb*, *Fo*, or a scrambled version of *Fo* pheromone were dissolved in 50% (v/v) MeOH at the concentration of 378 µM.

Horse Raddish peroxidase preparation (HRP)

Horse radish peroxidase (Sigma P-8375) was resuspended in phosphate-buffered saline buffer (PBS) at a concentration of 200 µM.

Dose-response curves and flow cytometry

Characterization of the fungal pheromones was done by conducting dose-response analyses following Jensen et al. protocol [8]. The same procedure was followed for studying the antagonist effect of a pheromone with one exception. The biosensor strains were first incubated with the candidate antagonist pheromone (priming), followed by the addition of the agonist pheromone after 15 minutes (competition). All data were acquired with the NovoCyte Quanteon™ (Agilent) flow cytometer. For each condition tested, four biological replicates were analyzed, with a threshold of 10,000 events per replicate.

Illumina

Illumina Library Preparation

Following Illumina's recommendation protocol, 50 ng of high-quality gDNA was used for a two-step PCR. PCR1 was set with 2.5 µl of gDNA, 5 µl of DOG129 (1µM), 5 µl of DOG130 (1µM), and 12.5 µl of 2x KAPA HiFi HotStart ReadyMix. A PCR clean-up was performed with AMPure XP beads (1.8 ratio) and EtOH 80%. Before performing PCR2, 1 µl of each reaction was run on a bioanalyzer DNA 1000 chip to verify the size of 395 bp. PCR2 was performed with 5 µl of DNA, 5 µl of Nextera XT Index Primer 1 (i701, i702, i703, i704, i705, i706, i707, i708, or i709), 5 µl of Nextera XT Index Primer 2 (i501), 2x KAPA HiFi HotStart ReadyMix 25 µl and 10 µl of Milli-Q water. A second PCR clean-up was performed with AMPure XP beads (1.8 ratio) and EtOH 80%. Library size validation (427 bp) was performed on a bioanalyzer DNA 1000 chip and DNA concentration was measured using Qubit 2.0. A pool of all samples was conducted to achieve a final DNA concentration of 10 nM with a proportion of 55 % YLP1 pre-enrichment and the remaining 45% with the equimolar concentration of all the remaining enriched samples.

Illumina Data Processing

The sample was sequenced with NextSeq 500 Mid Output 150 cycles with 4 technical replicates. Amplicon analysis was conducted with the standardized workflow Natrix [9]. In brief, FastQC (v0.11.9) was used to quality control the reads, and low-quality tails were removed from the reads using PRINSEQ [10] (v0.20.4). Trimmed reads with an average Phred score of less than 25 were discarded. DADA2 [11] (v1.18.0) was used to count the number of amplicon sequence variants (ASVs) and chimera detection was done by VSEARCH [12] (v2.15.2). DESeq2 [13] (v1.26.0) was used for variance-stabilizing transformation (VST) to normalize the read counts, and PCA and hierarchical clustering were used to detect any outliers. Since no outliers were detected, we combined the raw reads of the technical replicates and performed reads per million (RPM) normalization. Furthermore, we subtracted the RPM counts of the control starting library to allow for a better sample comparison. The data processing and ASV count analysis were done in Jupyter notebooks which can be found at https://github.com/Synthetic-Biology-Tools-for-Yeast/Yeast-Mating-Platform.

Quantification of fungal chemotropism

B. bassiana chemotropism was conducted as described previously by Turrà et al. with few modifications [14]. *B. bassiana* was revived in Oat Meal Agar (OMA) for a week. Spores were collected with water/glycerol 50% and stored at 4 °C. Spores were counted using a Neubauer chamber and dissolved to reach a concentration of 10^6 spores/ml. On the side glass microscope slides were sterilized and 3 lines were drawn on the back side of each slide: a scoring line in blu, a solvent line in blu, and a test compound in red. On the front side, 500 µl of water agar was added to create a thin layer in which 10 µl of test compound (378 µM of pheromone or water) and 10 µl of solvent (50% v/v methanol) were added in their

respective lines. 15 µl of spores were added on the scoring line and spread with a cover glass slide. After 20 hours the germination was assessed on a Leica DM4000 B microscope (Leica Microsystems) equipped with a DFC300 FX camera (Leica Microsystems).

Metabolomics of B. bassiana

B. bassiana DSM 62075 was cultivated at 25°C for 7 days onto YPD agar plates containing either MeOH, scrambled, *Bb,* or *Fo* pheromone. Afterward, agar pieces (6 mm diameter plugs) were cut off with a scalper and transferred to a glass vial containing a solvent mixture (MeOH:AcOEt:CH_2Cl_2 1:2:3 +0.1% (v/v) formic acid). Extractions were performed from three different biological replicates for all conditions. Samples were sonicated for 60 minutes and the supernatant was transferred to a new vial for complete solvent evaporation. Extracts were resuspended in HPLC grade MeOH for further UHPLC-HRMS/MS analyses.

Two methods were developed for UHPLC-HRMS/MS. Both platforms utilized a Vanquish Duo UHPLC binary system (ThermoFisher Scientific, Waltham, Massachusetts, USA.) coupled with an Orbitrap IDX™ mass spectrometer (ThermoFisher Scientific, Waltham, Massachusetts, USA.). The sample extracts were analyzed using two separated reverse phase LC-MS methods, one optimized for more hydrophilic (Method A, LC-MS/MS as previously described in [15]) and the other one for more hydrophobic compounds (Method B) using a Waters™ Acquity UPLC BEH C18 (5 cm × 2.1 mm, 1.7-mm) column equipped with an Acquity UPLC BEH C18 guard column kept at 70°C. The mobile phases consisted of MilliQ™ water + 10mM (v/v) ammonium acetate adjusted with NH4OH to reach pH=9 (A), and acetonitrile + 0.1% (v/v) formic acid (B) at a flow rate of 0.5 mL min^{-1}. The chromatographic gradient applied was as follows: 40% B held for 0.4 min, followed by a linear gradient to 100% B over 5.6 min and held for 2.5 min before going back to initial conditions (the re-equilibration time was 1.5 min). The injection volume was set at 1 mL. The MS(MS) measurements were done in positive-heated electrospray ionization (HESI) mode with a voltage of 3500 V, acquiring in full MS/MS spectra (data dependent acquisition-driven MS/MS) with a *m/z* range of 100–1500. The MS1 resolution was set at 120,000 and the MS2 resolution at 30,000. Precursor ions were fragmented by stepped high-energy collision dissociation (HCD) using collision energies of 20, 40, and 55. The automatic gain control (AGC) target value was set at 4×10^5 for the full MS and 5×10^4 for the MS/MS spectral acquisition.

The data preprocessing was performed using MZmine 2.53 [16,17] to generate a table of features. Output tables were submitted to the Global Natural Products Social Molecular Networking (GNPS-2) environment (https://gnps2.org/homepage), using the Feature-Based Molecular Networking (FBMN) workflow [18]. Processed network output was visualized and further edited with Cytoscape version 3.9.1.

Molecular dynamics (MD) simulation

GPCR and ligand complexes were predicted with AlphaFold2 Multimer [19] using ColabFold [20]. Receptor-ligand complexes predicted in a similar pose to *Sc*.Ste2 receptor-ligand complexes [21] were selected. Protein preparation and minimization, system setup, MD simulations, and data analysis were performed using Maestro (Schrödinger Release 2024-1). GPCRs were restricted to residues in the N-terminal and the transmembrane domains (1-291). The force field of the ligands was generated with LigPrep. GPCR-ligand complexes were prepared with the Protein Preparation Wizard (Sastri et al. 2013) at pH 5.6, which included capping GPCR chain termini with neutral acetyl and methylamide groups, assignment of histidine protonation states, and whole structure minimization. *F. oxysporum* pheromone does not establish intramolecular disulfide bonds [22], therefore the intramolecular disulfide bond was reduced for all ligands. The System Builder module was used to prepare the orthorhombic simulation box (10x10x10 Å), with the prepared GPCR-ligand complex embedded in a pre-equilibrated membrane (310K) palmitoyl-oleoyl-phosphatidylcholine (POPC) bilayer aligned with PPM3.0 of the OPM database alignment (Lomize et al. 2022), TIP3 solvent neutralized with 0.15 Na+/Cl- ions, and the OPLS4 force field (Lu et al. 2021). Membrane model system default relaxation was used to minimize the system, and the final snapshot was used to run five independent production runs with random seeds for each GPCR-ligand complex using Desmond (Bowers et al. 2006). Simulations were run at 300 K for 300 ns and snapshots were stored at every 500-ps interval. Aggregated MD data was analyzed with Jupyter Notebook and structural images were acquired with PyMol Molecular Graphics System version 2.5.0.

Data analysis and statistical analysis

Flow cytometry data and gating

All flow cytometry data were extracted as FCS files and gated in FlowLogic™ v8.3 (Inivai Technologies). For the biosensors assays P*FUS1-GFP*-based two gates were performed. The first on alive cells, and the second to exclude a small fraction (≈ 1%) of not responding cells [8]**.** Fluorescence data points were derived from gated populations' median values and median GFP fluorescence intensities. Normalized GFP intensity was obtained by normalizing it to the mean of the background.

Diploid frequency on plates

After the quantification of the haploid strains and diploids, the limiting haploid A was determined, and Eq. (1) was applied.

$$\text{Diploid frequency} = (\text{Diploids})/(\text{HaploidA}+\text{Diploids}) * 100 \qquad (1)$$

qPCR - diploid frequency

The relative quantification of diploids was performed by comparing the cycle threshold (Ct) value of the conserved regions (R1 and R3) flanking the barcodes and the Ct value of the amplicon generated with two barcodes. All possible combinations of barcodes plus 3 technical replicates of the control (DOG77 + DOG78) were tested. The relative quantification was calculated using ΔCt method [23,24].

$$2^{-\Delta CT} \qquad (2)$$

Where ΔCT = CT (barcodes) – CT (conserved region).

Data and statistical analysis

Data analysis, statistical analysis, and graphing were done in GraphPad Prism v10 (GraphPad Software), FlowLogic™ v8.3 (Inivai Technologies), and Jupyter Notebook. Sigmoidal dose-response curve fits were computed using nonlinear regression by the variable slope (four parameters) model in GraphPad Prism v10 (GraphPad Software), using default settings (Supplementary Data 3). The significance of the experiments was assessed by one-way or two-way ANOVA multivariate test and post-hoc analysis by Dunnett's or Tukey's multiple comparison test, respectively (Supplementary Data 3). All statistical tests were done in GraphPad Prism v10 (GraphPad Software) with a default 95% confidence interval ($\alpha = 0.05$) applied and multiplicity-adjusted *p* values were reported to account for all multiple comparisons within tests.

Non-targeted analysis of Metabolomic responses was performed by applying ANOVA simultaneous component analysis (ASCA) [25]. The following model for linking the experimental conditions (**A**), metabolomic responses (**Y**), and residuals (**E**) were applied in Eq. 3:

$$Y=A+E \tag{3}$$

Before any modeling, each MS dataset was scaled to unit variance. The ASCA model aimed at testing, if a significantly different metabolomic response could be identified based on the three levels of pheromone supplementations (Scramble, *Bb*, *Fo*) and the control with MeOH, assed across 4 different MS conditions (method A in positive mode, method A in negative mode, method B and all methods combined). The significance of pheromone supplementation was evaluated using permutation testing, with 10,000 permutations performed for each dataset. The significance level was set at 0.05 to compare the simulated null distribution against the observed effects. The results of the ASCA modeling process

were visualized by depicting the scores plots for each level of pheromone supplementations across all MS conditions (Supplementary Data 3). In addition, the ASCA model loadings, containing the mass fractions, were investigated, identifying which significantly contributed to the variation of pheromone supplements. This was done by removing all absolute loading values with confidence intervals containing 0 identified via bootstrapping. It should be noted that the bootstrapping confidence interval was estimated based on empirical distribution.

Flow cytometry settings

NovoCyte Quanteon™ (Agilent) settings

Excitation was done with a blue 488 nm laser for GFP. GFP emission was detected with a 530/30 nm BP filter (471 V), while FSC and SSC were detected with a 561/14 nm BP filter (400 V). The machine ran with a core diameter of 10.1 µm (24 µl/min), two mixing cycles every well (1500 g, Acc. = 1 s, Dur. = 10 s), one rinse cycle every well, and a threshold for event detection at >150,000 FSC-H. NovoFlow Solution (Agilent) was used and the machine was calibrated with NovoCyte QC Particles (Agilent).

References

1. Bitinaite, J. *et al.* USER™ friendly DNA engineering and cloning method by uracil excision. *Nucleic Acids Res.* **35**, 1992–2002 (2007).
2. Jessop-Fabre, M. M. *et al.* EasyClone-MarkerFree: A vector toolkit for marker-less integration of genes into Saccharomyces cerevisiae via CRISPR-Cas9. *Biotechnol. J.* **11**, 1110–1117 (2016).
3. Deichmann, M. *et al.* Engineered yeast cells simulating CD19+ cancers to control CAR T cell activation. *bioRxiv* 2023.10.25.563929 (2023) doi:10.1101/2023.10.25.563929.
4. Prins, R. C. & Billerbeck, S. A buffered media system for yeast batch culture growth.

BMC Microbiol. **21**, 127 (2021).

5. Gietz, R. D. & Schiestl, R. H. Quick and easy yeast transformation using the LiAc/SS carrier DNA/PEG method. *Nat. Protoc.* **2**, 35–37 (2007).
6. Jensen, E. D. *et al.* A synthetic RNA-mediated evolution system in yeast. *Nucleic Acids Res.* **49**, e88 (2021).
7. Wäneskog, M. *et al.* Heat pre-treatment reduces multiplicity of plasmid transformations in yeast during electroporation, without diminishing the transformation efficiency. *bioRxiv* 2024.07.03.601847 (2024) doi:10.1101/2024.07.03.601847.
8. Jensen, E. D. *et al.* Engineered cell differentiation and sexual reproduction in probiotic and mating yeasts. *Nat. Commun.* **13**, 6201 (2022).
9. Welzel, M. *et al.* Natrix: a Snakemake-based workflow for processing, clustering, and taxonomically assigning amplicon sequencing reads. *BMC Bioinformatics* **21**, 526 (2020).
10. Schmieder, R. & Edwards, R. Quality control and preprocessing of metagenomic datasets. *Bioinformatics* **27**, 863–864 (2011).
11. Callahan, B. J. *et al.* DADA2: High-resolution sample inference from Illumina amplicon data. *Nat. Methods* **13**, 581–583 (2016).
12. Rognes, T., Flouri, T., Nichols, B., Quince, C. & Mahé, F. VSEARCH: a versatile open source tool for metagenomics. *PeerJ* (2016) doi:10.7287/peerj.preprints.2409.
13. Love, M. I., Huber, W. & Anders, S. Moderated estimation of fold change and dispersion for RNA-seq data with DESeq2. *Genome Biol.* **15**, 550 (2014).
14. Turrà, D., El Ghalid, M., Rossi, F. & Di Pietro, A. Fungal pathogen uses sex pheromone receptor for chemotropic sensing of host plant signals. *Nature* **527**, 521–524 (2015).
15. Radi, M. S., Munro, L. J., Rago, D. & Kell, D. B. An untargeted metabolomics strategy to identify substrates of known and orphan E. coli transporters. *Membranes* **14**, (2024).
16. Pluskal, T., Castillo, S., Villar-Briones, A. & Oresic, M. MZmine 2: modular framework for processing, visualizing, and analyzing mass spectrometry-based molecular profile data. *BMC Bioinformatics* **11**, 395 (2010).

17. Schmid, R. *et al.* Integrative analysis of multimodal mass spectrometry data in MZmine 3. *Nat. Biotechnol.* **41**, 447–449 (2023).
18. Nothias, L.-F. *et al.* Feature-based molecular networking in the GNPS analysis environment. *Nat. Methods* **17**, 905–908 (2020).
19. Evans, R. *et al.* Protein complex prediction with AlphaFold-Multimer. *bioRxiv* 2021.10.04.463034 (2021) doi:10.1101/2021.10.04.463034.
20. Mirdita, M. *et al.* ColabFold: making protein folding accessible to all. *Nat. Methods* **19**, 679–682 (2022).
21. Velazhahan, V., Ma, N., Vaidehi, N. & Tate, C. G. Activation mechanism of the class D fungal GPCR dimer Ste2. *Nature* **603**, 743–748 (2022).
22. Vitale, S. *et al.* Structure-activity relationship of α mating pheromone from the fungal pathogen Fusarium oxysporum. *J. Biol. Chem.* **292**, 3591–3602 (2017).
23. Harshitha, R. & Arunraj, D. R. Real-time quantitative PCR: A tool for absolute and relative quantification. *Biochem. Mol. Biol. Educ.* **49**, 800–812 (2021).
24. Schmittgen, T. D. & Livak, K. J. Analyzing real-time PCR data by the comparative CT method. *Nat. Protoc.* **3**, 1101–1108 (2008).
25. Smilde, A. K. *et al.* ANOVA-simultaneous component analysis (ASCA): a new tool for analyzing designed metabolomics data. *Bioinformatics* **21**, 3043–3048 (2005).